

Design of Maisel sidelobe blankers with a guarantee on the gap to optimality

ISSN 1751-8784
Received on 14th November 2015
Revised 18th February 2016
Accepted on 3rd April 2016
E-First on 21st June 2016
doi: 10.1049/iet-rsn.2015.0572
www.ietdl.org

Osman Coşkun¹ ✉, Çağatay Candan¹

¹Department of Electrical and Electronics Engineering, Middle East Technical University (METU), Ankara, Turkey
✉ E-mail: osmanc@gmail.com

Abstract: The conventional sidelobe blanking system, known as the Maisel sidelobe blanker, uses two receiving channels with different gains to detect the presence of a jammer. The Maisel system is an *ad-hoc* detector without any optimality properties. Yet, it has been successfully utilised in numerous operational systems. Here, the authors study the optimum Neyman–Pearson type sidelobe blanking (SLB) detectors for the Swerling target models to assist the design of Maisel blankers. The authors note that the optimal sidelobe blankers are of theoretical interest, since they require the knowledge of target and jammer parameters, which are typically not available at the radar site. The main goals of the present study are (i) to derive the optimal Neyman–Pearson detectors for SLB, (ii) to examine the performance gap between the optimal and Maisel detectors, and (iii) to develop objective criteria for the design of Maisel blankers that provides a guarantee on the gap to the optimality. Ready-to-use computer programs to assist the design process are also provided.

1 Introduction

Signals intercepted from the antenna sidelobes can cause false target declarations, reduced tracking accuracy, reduced direction finding accuracy, and other undesired effects. To reduce the impact of such effects, a sidelobe blanking (SLB) architecture, known as the Maisel structure, has been proposed [1]. The Maisel structure uses two receiving channels. The first one is the main channel whose antenna has high gain in the main beam and low gain in the sidelobes. The second channel is called the auxiliary channel and has an omnidirectional pattern, i.e. a flat gain which is typically slightly greater than the sidelobe gain of the main antenna as illustrated in Fig. 1.

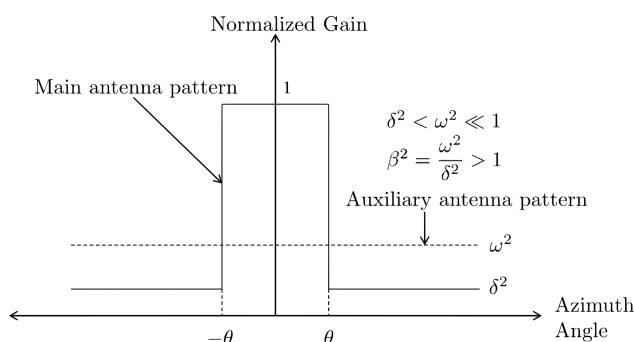


Fig. 1 Gain patterns of main and auxiliary antennas for a conventional SLB system

The Maisel structure generates a blanking signal when the ratio of the auxiliary channel output power (v) to main channel output power (u), that is (v/u), is greater than blanking threshold F as shown in Fig. 2. A blanking decision disables the main channel. Stated differently, the main channel output is discarded without any further processing upon blanking. It should be clear that an erroneous blanking decision causes a degradation in the performance detection. The main goal of sidelobe blanker design is to reliably detect the presence of a sidelobe jammer with a minor loss in the target detection capabilities.

As shown in Fig. 1, the gain of the omnidirectional antenna (ω^2) should satisfy the condition $\omega^2/\delta^2 = \beta^2 \geq 1$ for a reliable operation. Stated differently, the auxiliary antenna acts as a better receiver in comparison to the main antenna for the targets in the sidelobe region. An interfering signal in the sidelobe region with the power α produces main and auxiliary channel output powers of $\delta^2\alpha$ and $\omega^2\alpha$, respectively. The ratio of auxiliary to main channel output, the decision statistics for the Maisel detector, is β^2 and this ratio is to be compared with the threshold F . Therefore $\beta^2 \geq F$ condition is required to successfully blank the sidelobe interferer [1]. Similarly, in order not to erroneously blank a target in the main lobe region, which produces auxiliary to main channel output ratio of ω^2 , the condition of $\omega^2 \leq F$ is also required, [1]. As a summary, the following three conditions are typically required for the design of Maisel sidelobe blankers:

- i. $\beta^2 = (\omega^2/\delta^2) \geq 1$,
- ii. $\beta^2 \geq F$,

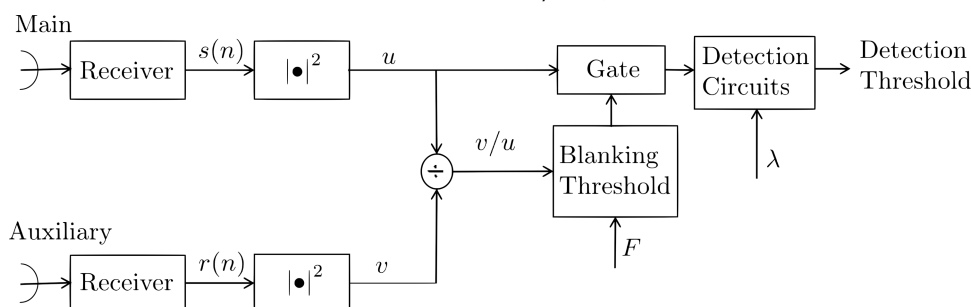


Fig. 2 Block diagram of Maisel sidelobe blanker [1]

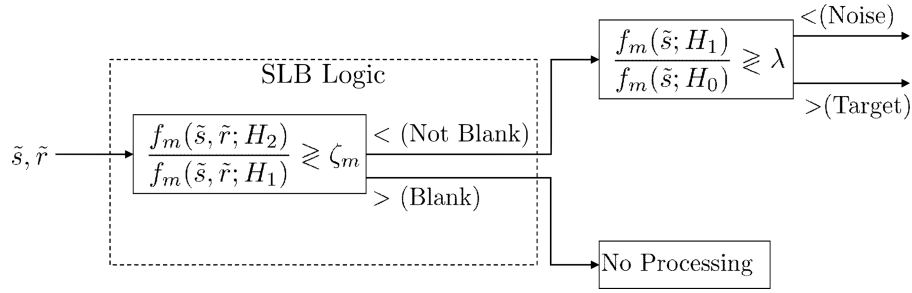


Fig. 3 Illustration of two-stage radar receiver with a sidelobe blanker logic

iii. $\omega^2 \leq F$.

It should be noted that these conditions are rather naive, since their derivation is based on noise free operation, that is the statistical variations due to noise, target fluctuations and so on are not taken into account. Typically, these conditions are interpreted as the *necessary conditions* for the design of Maisel SLB systems; but they do not guarantee a satisfactory performance in practical scenarios. In practice, to realise a good performance in the presence of noise and other statistical variations, the parameters β^2 , ω^2 , and F are chosen such that the conditions are satisfied with some margin. To the extent of our knowledge, there is no quantitative study on the optimality of Maisel scheme and there is no work on the selection of parameters with the guidance of the optimal Neyman–Pearson test. This study aims to fill this gap in the literature.

The classical SLB systems are well studied in the literature. In [2], Farina examines the classical SLB system in detail and derives the probability of blanking the jammer in sidelobe (P_b), the probability of blanking the target in main beam (P_{tb}), and the probability of false target due to jammer in sidelobe (P_{ft}) for Swerling-0 target model. In [3], Farina and Gini extends the aforementioned probability calculation to the Swerling-1 targets. The work is extended to gamma distribution with an arbitrary shape parameter, and shadowed rice target models [4] and the effects of correlated Gaussian clutter in addition to thermal noise is also accounted in [5]. Shnidman and Toumodge [6] give the analysis of an arbitrary number of non-coherently integrated pulses for the case of non-fluctuating and gamma fluctuating target. Shnidman and Shnidman [7] extend the analysis to non-central gamma (NCG) and NCG-gamma fluctuations. In [8], Cui *et al.* give the performance assessment for arbitrary correlated, possibly non-identically distributed, fluctuating target and/or jamming returns for a given number of integrated pulses.

To the best of our knowledge, in spite of several important works on the Maisel structure, its performance gap from the optimal detector is not studied in the literature. In [9], Finn *et al.* note that the SLB systems derived from the Neyman–Pearson likelihood ratio test (LRT) are hard to implement in real time and the Maisel structure is suggested as a substitute detector with a simple implementation. One of our goals is to justify the good performance of properly designed Maisel SLB systems by conducting a comparison with the optimal Neyman–Pearson detector. It should be mentioned that the optimal Neyman–Pearson test is not possible to implement in practice; since the optimal Neyman–Pearson detector requires several jammer and target parameters which are not typically available to the radar operator. Therefore, our goal is *not* to suggest a practical alternative SLB structure; but to examine the performance gap between the Maisel and optimal system for different scenarios, to identify the conditions that Maisel system operates in the close vicinity of the optimal system and, finally, to present some objective criteria to the designers of Maisel blankers to achieve almost optimal performance.

2 Neyman–Pearson type optimal sidelobe blankers

Let \tilde{s} and \tilde{r} denote the complex valued matched filtered outputs of the main and auxiliary channels at a specific time. We have three hypotheses, namely noise only (H_0), target in main lobe and no jammer in sidelobe (H_1), and jammer in sidelobe and no target in main lobe (H_2)

$$H_0: \begin{cases} \tilde{s} = \tilde{w}_s \\ \tilde{r} = \tilde{w}_r \end{cases} \quad (1)$$

$$H_1: \begin{cases} \tilde{s} = a_0 \exp(j\phi_a) + \tilde{w}_s \\ \tilde{r} = \omega a_0 \exp(j\phi_a) + \tilde{w}_r \end{cases} \quad (2)$$

$$H_2: \begin{cases} \tilde{s} = c_0 \exp(j\phi_c) + \tilde{w}_s \\ \tilde{r} = \beta c_0 \exp(j\phi_c) + \tilde{w}_r \end{cases} \quad (3)$$

Here $\tilde{a} = a_0 \exp(j\phi_a)$ and $\tilde{c} = c_0 \exp(j\phi_c)$ indicate target and jammer voltage signal and $\tilde{w}_s \sim \mathcal{CN}(0, \sigma^2)$ and $\tilde{w}_r \sim \mathcal{CN}(0, \sigma^2)$ denote receiver noise in main and auxiliary channels, respectively. $\mathcal{CN}(0, \sigma^2)$ represents zero mean complex circularly symmetric Gaussian random variables with σ^2 variance. Note that the phrase ‘jammer’ in this work also applies to an interfering target in the sidelobe.

We assume that phases of target and jammer signals are independent of each other. The receiving channels are perfectly matched [This assumption brings the coherency between receiving channels and only affects the design of optimal detectors which are studied to provide a performance bound for the Maisel blankers.]. Namely, $E[\tilde{r}\tilde{s}^*; H_1] = \omega E[|a_0|^2]$ and $E[\tilde{r}\tilde{s}^*; H_2] = \beta E[|c_0|^2]$. The LRT to decide blanking the main channel can be formed as follows:

$$\Lambda_m(\tilde{s}, \tilde{r}) = \frac{f_m(\tilde{s}, \tilde{r}; H_2)}{f_m(\tilde{s}, \tilde{r}; H_1)} \underset{\text{Blank}}{\overset{\text{Blank}}{\geq}} \zeta_m, \quad m = 0, 1, 3. \quad (4)$$

Here, $f_m(\tilde{s}, \tilde{r}; H_2)$ and $f_m(\tilde{s}, \tilde{r}; H_1)$ are the joint probability density functions (pdf) of \tilde{s} and \tilde{r} , respectively, for Swerling- m ($m = 0, 1, 3$) target model and the Blank and $\overline{\text{Blank}}$ denote the blanking and not-blanking decisions, respectively. It should be noted that the sidelobe blanker logic given by (4) forms the first stage of the detector shown in Fig. 3.

The sidelobe blanker logic shown in Fig. 3 generates the decision test which is compared with the threshold ζ_m . If the threshold is exceeded, the main channel is no longer processed and a jammer decision is declared. If the first stage declares the absence of jammer, the main channel output is further processed for the presence or absence of a target.

It can be shown that the sidelobe blanker logic, the first stage of the detector in Fig. 3, has the optimality properties in the sense that given a fixed probability of (erroneously) blanking the target signal, $\Pr(\text{Blank}|H_1)$, the probability of blanking the jammer signal is maximised, $\Pr(\text{Blank}|H_2)$, with the shown two-stage test. The proof for this claim is given in Appendix 1. With the adoption of this optimality result, the blanking process and target detection process can be separated.

In the rest of this section, the log LRTs (LLRTs) of hypotheses H_2 and H_1 are calculated for different target fluctuations models. We denote the decision statistics for this purpose as

$$d_m = \log \Lambda_m(\tilde{s}, \tilde{r}) \underset{\text{Blank}}{\overset{\text{Blank}}{\geq}} \eta_m, \quad m = 0, 1, 3. \quad (5)$$

Here d_m is the decision statistics for the Swerling- m target model. The probability for the undesired event of (erroneous) target blanking probability $P_{\text{tb}} = \Pr(\text{Blank} | H_1) = \int_{\eta_m}^{\infty} f_{d_m | H_1}(x) dx$ can be set to a predefined value by adjusting the threshold level. As shown, the threshold value becomes a function of the parameters $\{\text{SNR}, \text{JNR}, \omega^2, \beta^2\}$. After setting the threshold, the probability of the desired event, that is the probability of blanking an active jammer, can be determined as $P_b = \Pr(\text{Blank} | H_2) = \int_{\eta_m}^{\infty} f_{d_m | H_2}(x) dx$. In the following subsections, we present the details of these calculations.

2.1 Swerling-1 target model

Swerling-1 target model assumes the amplitude of target return, $a_0 = |\tilde{a}|$, is Rayleigh and the phase ϕ_a is uniformly distributed over $(0, 2\pi)$. Also, there is no pulse-to-pulse fluctuation in one antenna scan. This model is referred to as scan-to-scan fluctuation. The magnitude of \tilde{a} is distributed as [10]

$$f(a_0) = \frac{2a_0}{\sigma_a^2} \exp\left(-\frac{a_0^2}{\sigma_a^2}\right), \quad a_0 \geq 0. \quad (6)$$

Note that average power of target return signal is σ_a^2 and is complex Gaussian distributed having a variance of σ_a^2 , that is, $\tilde{a} \sim \mathcal{CN}(0, \sigma^2)$. The signal-to-noise-ratio (SNR) and jammer-to-noise-ratio (JNR) are defined as

$$\text{SNR} = \gamma_s = \frac{|\tilde{a}|^2}{E[w_s^2]} = \frac{\sigma_a^2}{\sigma^2}, \quad (7)$$

$$\text{JNR} = \gamma_j = \frac{|\tilde{c}|^2}{E[w_s^2]} = \frac{\sigma_c^2}{\sigma^2}. \quad (8)$$

The LLRT to decide blanking or not [11]

$$d_1 = A|\tilde{s}|^2 + B|\tilde{r}|^2 + C2\text{Re}(s\tilde{r}^*) \underset{\text{Blank}}{\overset{\text{Blank}}{\geq}} \eta_1, \quad (9)$$

where

$$A = \frac{\gamma_s \omega^2 + 1}{\gamma_s(1 + \omega^2) + 1} - \frac{\gamma_j \beta^2 + 1}{\gamma_j(1 + \beta^2) + 1}, \quad (10)$$

$$B = \frac{\gamma_s + 1}{\gamma_s(1 + \omega^2) + 1} - \frac{\gamma_j + 1}{\gamma_j(1 + \beta^2) + 1}, \quad (11)$$

$$C = \frac{-\omega\gamma_s}{\gamma_s(1 + \omega^2) + 1} - \frac{\beta\gamma_j}{\gamma_j(1 + \beta^2) + 1}. \quad (12)$$

The test given in (9) can also be expressed as $d_1 = \mathbf{x}^H(\mathbf{C}_1^{-1} - \mathbf{C}_2^{-1})\mathbf{x}$ where \mathbf{C}_1 and \mathbf{C}_2 are the covariance matrices of the two dimensional Gaussian random vector $\mathbf{x} = [\tilde{s} \ \tilde{r}]$ for different hypotheses and defined as follows (see [11] for further details)

$$\mathbf{C}_i = E[\mathbf{x}\mathbf{x}^H; H_i] = \begin{bmatrix} E[|\tilde{s}|^2; H_i] & E[\tilde{s}\tilde{r}^*; H_i] \\ E[\tilde{s}^*\tilde{r}; H_i] & E[|\tilde{r}|^2; H_i] \end{bmatrix}, \quad i = \{1, 2\}. \quad (13)$$

The pdf of the test statistic d_1 can be analytically expressed as [11–13]

$$f_{d_1}(d_1) = \begin{cases} \frac{ab}{a+b} \exp(-ad_1), & d_1 \geq 0 \\ \frac{ab}{a+b} \exp(bd_1), & d_1 < 0 \end{cases}. \quad (14)$$

The parameters a and b appearing in (14) are defined through a rather complicated functions of $\mu_{\tilde{r}\tilde{s}}$ and r , [14]

$$a = \sqrt{r^2 + \frac{1}{4(\mu_{\tilde{r}\tilde{r}}\mu_{\tilde{s}\tilde{s}} - |\mu_{\tilde{s}\tilde{r}}|^2)(|C|^2 - AB)}} - r, \quad (15)$$

$$b = \sqrt{r^2 + \frac{1}{4(\mu_{\tilde{r}\tilde{r}}\mu_{\tilde{s}\tilde{s}} - |\mu_{\tilde{s}\tilde{r}}|^2)(|C|^2 - AB)}} + r \quad (16)$$

where $\mu_{\tilde{r}\tilde{s}} = (1/2)E[\tilde{r}\tilde{s}^*]$ and

$$r = \frac{A\mu_{\tilde{r}\tilde{r}} + B\mu_{\tilde{s}\tilde{s}} + C^*\mu_{\tilde{s}\tilde{r}} + C\mu_{\tilde{r}\tilde{s}}}{4(\mu_{\tilde{r}\tilde{r}}\mu_{\tilde{s}\tilde{s}} - |\mu_{\tilde{s}\tilde{r}}|^2)(|C|^2 - AB)}.$$

Threshold calculation: The threshold η_1 for the Neyman–Pearson test can be calculated from (14). For a given target blanking probability (P_{tb}), the threshold η_1 is

$$\eta_1 = \begin{cases} -\frac{1}{a} \ln\left[\left(\frac{a+b}{b}\right)P_{\text{tb}}\right], & P_{\text{tb}} \geq \frac{b}{a+b} \\ \frac{1}{b} \ln\left[-\left(\frac{a+b}{a}\right)(P_{\text{tb}} - 1)\right], & P_{\text{tb}} \leq \frac{b}{a+b} \end{cases}. \quad (17)$$

Blanking probability calculation: Using the threshold η_1 , the probability of blanking the jammer in sidelobe is

$$P_b = \begin{cases} \frac{b}{a+b} \exp(-a\eta_1), & \eta_1 \geq 0 \\ \frac{a}{a+b}(1 - \exp(b\eta_1)) + \frac{b}{a+b}, & \eta_1 \leq 0 \end{cases}. \quad (18)$$

Further details are given in Appendix 2.

2.2 Swerling-0 and Swerling-3 target models

Swerling-0 target model assumes that the phase of \tilde{a} (ϕ_a) is uniformly distributed over $(0, 2\pi)$ and the magnitude of \tilde{a} is deterministic. After forming the LRT and ignoring non-data dependent terms, we reach the following test:

$$d_0 = \frac{I_0((2c_0/\sigma^2)|\tilde{s} + \beta\tilde{r}|)}{I_0((2a_0/\sigma^2)|\tilde{s} + \omega\tilde{r}|)} \underset{\text{Blank}}{\overset{\text{Blank}}{\geq}} \eta_0. \quad (19)$$

where $I_0(\cdot)$ denotes the modified Bessel function of the first kind.

Swerling-3 target model is similar to the Swerling-1 model (scan-to-scan fluctuation) case except that the magnitude of \tilde{a} is distributed as [10]

$$f(a_0) = \frac{8a_0^3}{\sigma_a^4} \exp\left(-\frac{a_0^2}{\sigma_a^2}\right), \quad a_0 \geq 0. \quad (20)$$

After obtaining the joint pdf's of \tilde{s} and \tilde{r} (see Appendix 2 for derivations), the LLRT can be found as

$$d_3 = \mathbf{x}^H(\mathbf{C}_1^{-1} - \mathbf{C}_2^{-1})\mathbf{x} + \log\left(\frac{1 + \mathbf{x}^H(-\mathbf{C}_2^{-1} + \mathbf{I})\mathbf{x}}{1 + \mathbf{x}^H(-\mathbf{C}_1^{-1} + \mathbf{I})\mathbf{x}}\right) \underset{\text{Blank}}{\overset{\text{Blank}}{\geq}} \eta_3. \quad (21)$$

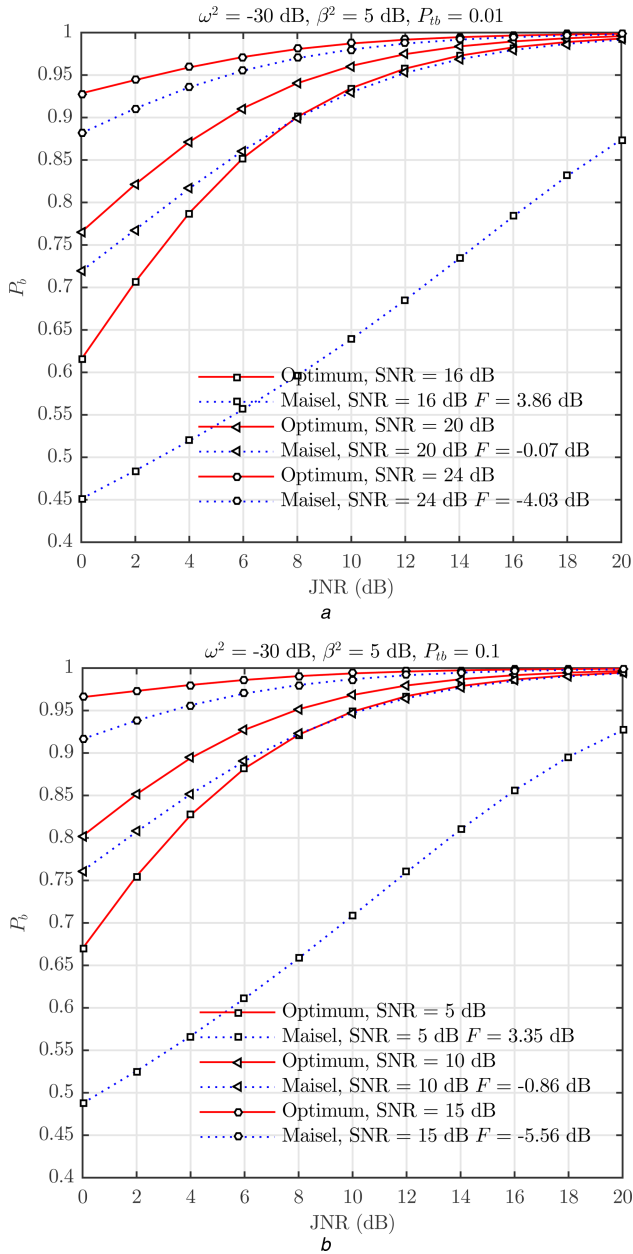


Fig. 4 Comparison of P_b on JNR for Swerling-1 targets. Parameters: $\beta^2 = 5$ dB, $\omega^2 = -30$ dB
(a) $P_{tb} = 0.01$, (b) $P_{tb} = 0.1$

where \mathbf{C}_1 and \mathbf{C}_2 are the covariance matrices defined in (13).

Due to the non-linearities present in d_0 and d_3 , the decision statistics for these tests are analytically formidable to obtain. We resort to the Monte Carlo methods for the assessment of these models. Some further details on the derivations are given in Appendix 2.

3 Performance comparison of Maisel structure and optimal detectors

We present a quantitative critique of the Maisel detector by conducting a comparison with the optimal detector for different target models. The optimal tests for Swerling targets given in (9), (19), and (21) depend on several parameters including operating SNR and JNR. Hence, the optimality, in the sense of Neyman–Pearson, is achieved through the knowledge target and jammer specific parameters which are not utilised in the classical Maisel SLB system. The performance superiority of the Neyman–Pearson detectors can be attributed to this additional knowledge. In practice, it may not be possible to reliably estimate SNR and JNR values on-the-fly and resorting to classical Maisel structure is

unavoidable. Yet, the performance gap between the optimal and Maisel structures, in spite of the unavailable information for the conventional structure, is the main interest of this section.

In the following subsections, we present a numerical comparison of Maisel structure and the optimal detector for three different Swerling models. It is assumed that both systems are equipped with an antenna having identical ω^2 and β^2 values. Both detectors are adjusted to meet a given target blanking (false blanking) probability.

3.1 Swerling-1 target model

Fig. 4a compares the performance of two systems at a fixed probability of target blanking. The target blanking probability is set to 0.01 and β^2 is chosen as 5 dB. The threshold values for Maisel detector at different SNR values are denoted in the figure legend. (the statistics of Maisel SLB are given in [3].) We note that threshold values for the optimum SLB detector depends on JNR; hence the threshold varies for each point given in Fig. 4a for the optimal test.

It can be noted from Fig. 4a that the performance gap between Maisel structure and optimum detector is large at SNR = 16 dB. For this case, the threshold F for Maisel structure is comparable with β^2 value. The other cases have much smaller performance gap between optimal test and Maisel structure. It can be noted that the performance gap diminishes as the threshold F of the Maisel structure gets smaller in comparison to β^2 .

Fig. 4b presents the result of an identical comparison for a higher target blanking of $P_{tb} = 0.1$. For the given P_{tb} value, the case of $F \approx \beta^2$ occurs at much smaller SNR values, i.e. SNR ≈ 5 dB. It can be noted that the cases for which the condition $F \ll \beta^2$ is satisfied, the performances of Maisel structure and the optimal detector are very similar. This general conclusion is indeed expected; but results given here quantitatively illustrate the performance gap from the optimal detector for different F and β^2 values. In the following section, we present a design guideline on how to make use of the presented results for the design of almost optimal Maisel sidelobe blankers.

3.2 Swerling-3 target model

The test given in (21) is the optimum Neyman–Pearson test for Swerling-3 targets. As in Swerling-1 case, the threshold η_3 in (21) depends on several parameters, including SNR, JNR, ω^2 , and β^2 . Swerling-3 target model corresponds to medium fluctuation between Swerling-1 and Swerling-0 target models. Since the fluctuation is less than Swerling-1 case, we can achieve the same probability of false blanking (P_{tb}) at lower SNR values.

Fig. 5 compares the two systems when β^2 is set to 5 dB. The results are similar to the Swerling-1 case. Due to less fluctuation compared with Swerling-1 target, the threshold values (F) and η_3 are smaller in comparison with Swerling-1 case. This results in a higher probability of blanking at the same JNR values than the one of Swerling-1 targets. It can be noted that when the main requirement of Maisel structure $F \ll \beta^2$ is satisfied, the performance of Maisel structure converges to the optimum SLB detector at even low JNR values. When this requirement is not satisfied, the performance of Maisel structure has a large gap from the optimal test, as in the Swerling-1 case.

3.3 Swerling-0 target model

The test given in (19) is the optimal Neyman–Pearson test for Swerling-0 targets. Fig. 6a compares the two systems for the false blanking probability (P_{tb}) of 0.01. The corresponding threshold values are shown in the figure legend. As in the Swerling-1 case, the Maisel structure behaves poorly when F is not sufficiently smaller than β^2 . It can be noted that, the performance gap gets smaller when JNR increases. Fig. 6b shows the identical comparison when the false blanking probability is increased to 0.05.

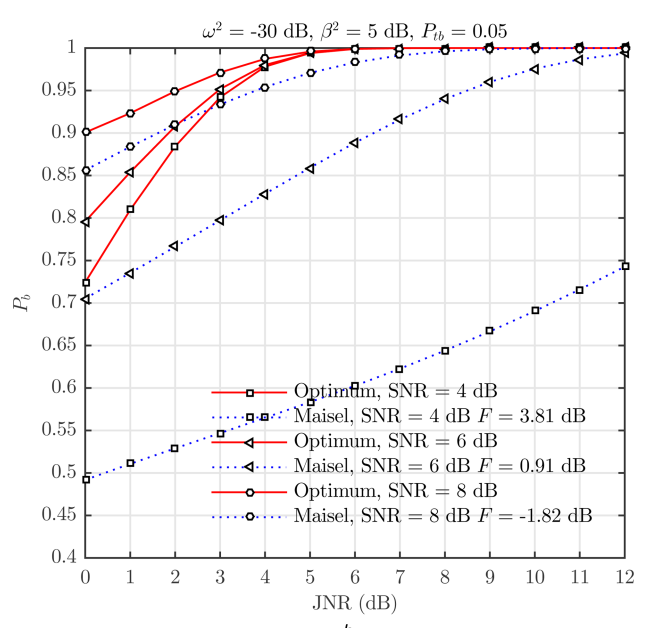
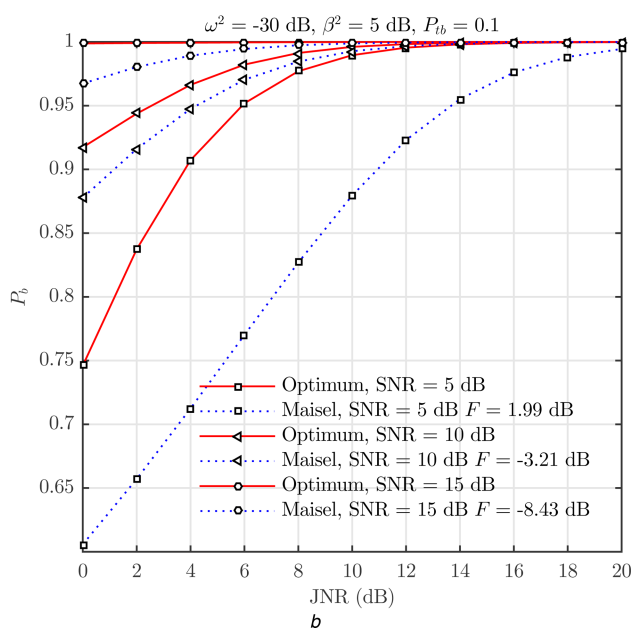
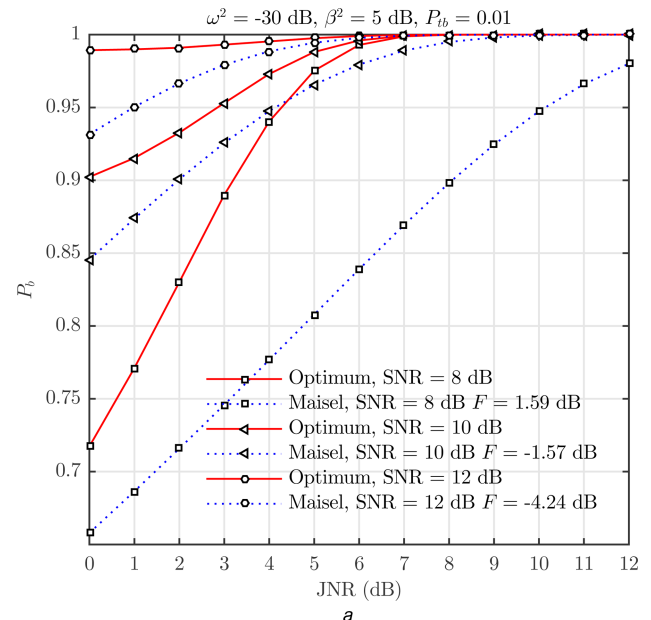
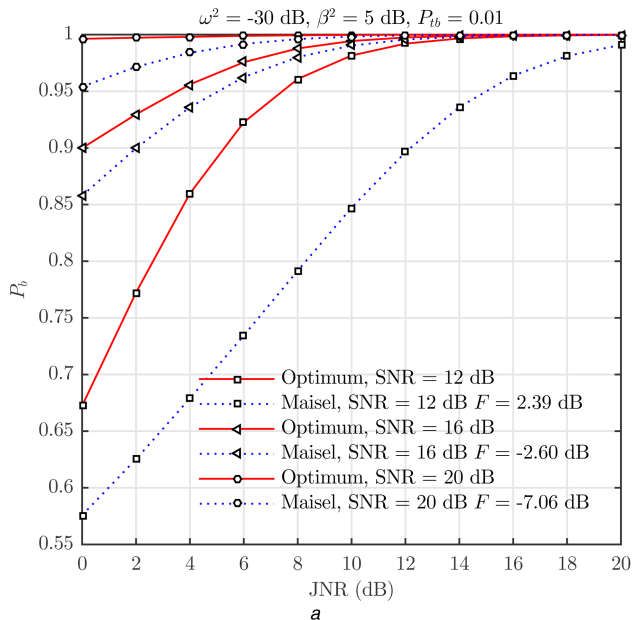


Fig. 5 Comparison of P_b on JNR for Swerling-3 targets. Parameters: $\beta^2 = 5$ dB, $\omega^2 = -30$ dB, and number of Monte Carlo trials = 10^6 (a) $P_{tb} = 0.01$, (b) $P_{tb} = 0.1$

Fig. 6 Comparison of P_b on JNR for Swerling-0 targets. Parameters: $\beta^2 = 5$ dB, $\omega^2 = -30$ dB, and number of Monte Carlo trials = 10^6 (a) $P_{tb} = 0.01$, (b) $P_{tb} = 0.05$

It can be noted that optimum SLB structure achieves higher blanking probability at a relatively smaller JNR values when compared with Swerling-1 and Swerling-3 cases. This is, indeed, expected due to the assumption of non-fluctuating target model.

4 Design of Maisel type SLB systems with an optimality guarantee

In the design of the Maisel sidelobe blankers, there are mainly two parameters, namely F and β^2 to be determined to achieve the desired blanking probability (P_b) at the expense of a fixed (erroneous) target blanking probability (P_{tb}). In this section, we aim to illustrate the process of designing Maisel type blankers with an optimality guarantee.

We illustrate the design process through a numerical example. In this example, a jammer with a JNR of 5 dB is assumed to be located in the sidelobe region. (It should be noted that the mentioned JNR values are the receiver JNR values, that is after the suppression of the jammer by the main antenna.) Our design goal is to blank the jammer with a probability of larger than 90% and the

tolerable erroneous target blanking probability should be at most to 5% for Swerling-1 targets.

Fig. 7 shows the performance comparison of Maisel type and optimal sidelobe blanker systems for different values of antenna gain margin (β^2) under the conditions of $P_{tb} = 0.05$, JNR = 5 dB. From this figure, we can see that when $\beta^2 = 10$ dB, the Maisel SLB provides a blanking probability (P_b) of 0.9, 0.95, and 0.97 when the threshold F is adjusted for the erroneous blanking of targets having SNR values 9, 12 and 15 dB, respectively. Hence, if the weakest target (target of lowest SNR) to be detected has an SNR of 9 dB, then it is necessary to have $\beta^2 = 10$ dB. If the weakest target SNR is around 12 dB, $\beta^2 = 7$ dB suffices to achieve the design goals.

It should be noted that a reduction in β^2 is equivalent to a relaxation in the main antenna sidelobe specifications. Hence, the utilisation of a smaller β^2 values is desirable from the viewpoint of antenna design. If the weakest target has an SNR value of 9 dB and $\beta^2 = 7$ dB, there exists a large gap between the performance of Maisel detector and optimal detector as illustrated by the vertical double sided arrows in Fig. 7. It can be noted that even a single

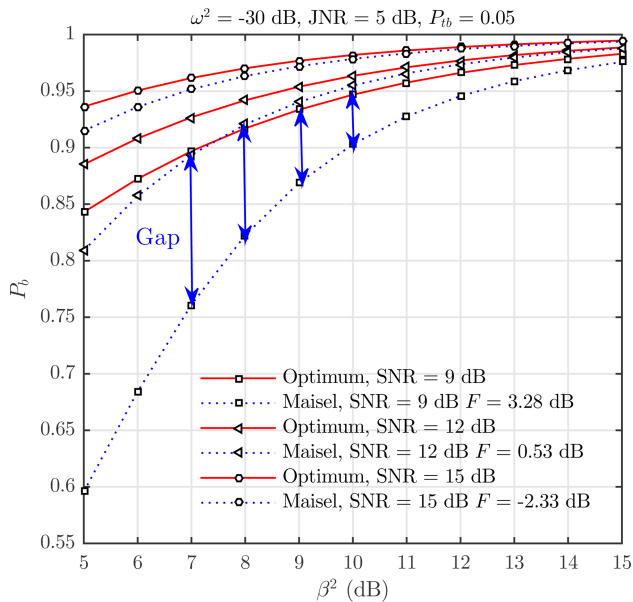


Fig. 7 Comparison of P_b on β^2 for Swerling-1 targets. Parameters: $P_{tb} = 0.05$, $JNR = 5$ dB, and $\omega^2 = -30$ dB

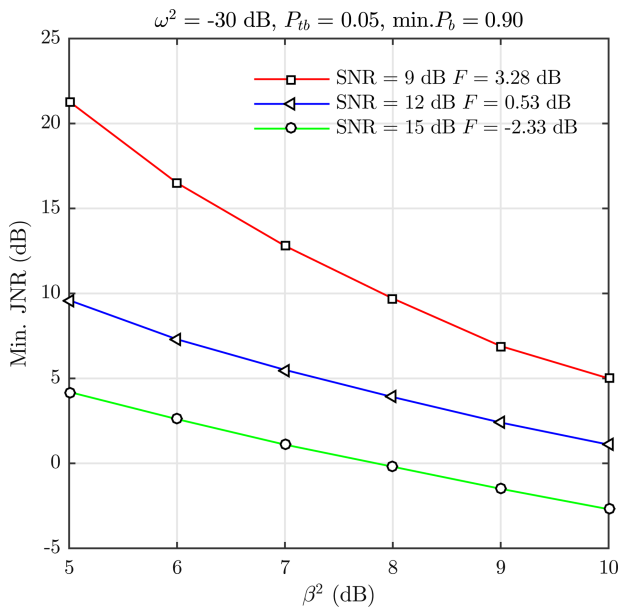


Fig. 8 Maisel minimum required JNR for different β^2 values (Swerling-1 target). Parameters: $P_{tb} = 0.05$, $\omega^2 = -30$ dB, and $\min. P_b = 0.90$

decibel in increase of β^2 from 7 to 8 dB, results in a significant reduction of this gap. Hence, an SLB designer, whose operational scenario includes target SNR values of 9 dB, can rightfully request an effort in the reduction of main antenna sidelobes. If the lowest target SNR values are around 12 dB, the gap between Maisel and optimal detector curves (shown with the triangle marker) is rather small and having a reduction in the main antenna sidelobe levels has a much smaller pay off in terms of the blanking probability.

To further assist the design process, we present the relation between minimum JNR and β^2 in Fig. 8. The JNR values shown in this figure is the smallest JNR value for which the design criteria are satisfied. Hence, this figure can be interpreted as the blanking effectiveness of the system as a function of β^2 . The desired probability of blanking (P_b) is set to 0.90, the erroneous target blanking probability is limited to 0.05, $P_{tb} \leq 0.05$ also in this figure. The curves given in Fig. 8 show the required JNR value for a fixed β^2 so that the probability gap between Maisel detector and optimal detector is smaller than 0.05. (The mentioned probability gap is illustrated with the double sided arrows in Fig. 7.) Hence, these

points on the curves shown in Fig. 8 refer to the Maisel systems whose performance has a fixed gap from the optimal detectors.

The curve with the square marker shows the case of weakest target SNR values of 9 dB. For this case, as noted earlier, $\beta^2 = 10$ dB is required to blank the jammers with receiver JNR of 5 dB with the desired blanking probability of 90%. For the same case, if β^2 happens to be 7 dB, the jammers with 13 dB JNR or higher can be blanked with the desired probability. As can be noted from Fig. 8, an increase in β^2 from 7 to 8 dB, results in the blanking of the jammers with $JNR > 10$ dB with the desired probability. Another dB increment further reduces this JNR value to 7 dB. It can be said that from this figure, the improvement in blanking effectiveness resulting for a single dB increment in β^2 can be read for the Maisel detectors with a fixed case worst case gap from the optimal detectors. Using these curves, a sidelobe blander designer can assess the return for the reduction of main antenna sidelobe levels in terms of blanking effectiveness.

To further assist the designer, we provide a set of ready-to-use, general purpose MATLAB programs to generate similar figures for different values of parameters such as P_{tb} , P_b , ω^2 and so on in [15].

5 Conclusion

The main goals of this study are to compare the performance of the Maisel SLB structure with the optimal detectors and to provide design guidance for the Maisel systems. To this aim, optimal Neyman–Pearson detectors are studied for Swerling-0, Swerling-1, and Swerling-3 target models. Unfortunately, the optimal detectors are not feasible to implement, since they require SNR and JNR values which are typically not available to the radar operator. Yet, the performance of the optimal detectors can be interpreted as a performance upper bound for the Maisel systems. One of the main goals of this study is to derive the mentioned performance bounds and examine the performance gap between the optimal detector and Maisel structure. A second goal is to develop design criteria and tools for the Maisel systems that guarantee a final design with a fixed performance gap from the optimal detectors. To this aim, the return in terms of jamming effectiveness as a function of β^2 is studied. More specifically, the return of a single dB increase in β^2 in terms of an increase in the blanking probability or a reduction in the minimum successfully blanked JNR level is examined. A general purpose MATLAB code to assist the design process is provided. Through the utilisation of the presented criteria and provided software, a sidelobe blander designer can easily assess the value of an increase in β^2 for different operational scenarios and design Maisel systems with a provable optimality guarantee.

6 References

- [1] Maisel, L.: 'Performance of sidelobe blanking systems', *IEEE Trans. Aerosp. Electron. Syst.*, 1968, **4**, (2), pp. 174–180
- [2] Farina, A.: 'Antenna-based signal processing techniques for radar systems' (Artech House Boston, 1992)
- [3] Farina, A., Gini, F.: 'Calculation of blanking probability for the sidelobe blanking for two interference statistical models', *IEEE Signal Process. Lett.*, 1998, **5**, (4), pp. 98–100
- [4] De Maio, A., Farina, A., Gini, F.: 'Performance analysis of the sidelobe blanking system for two fluctuating jammer models', *IEEE Trans. Aerosp. Electron. Syst.*, 2005, **41**, (3), pp. 1082–1091
- [5] Farina, A., Gini, F.: 'Design of SLB systems in the presence of correlated ground clutter', *Proc. IEE Radar Sonar Navig.*, 2000, **147**, (4), pp. 199–207
- [6] Shnidman, D., Toumodge, S.: 'Sidelobe blanking with integration and target fluctuation', *IEEE Trans. Aerosp. Electron. Syst.*, 2002, **38**, pp. 1023–1037
- [7] Shnidman, D., Shnidman, N.: 'Sidelobe blanking with expanded models', *IEEE Trans. Aerosp. Electron. Syst.*, 2011, **47**, pp. 790–805
- [8] Cui, G., De Maio, A., Piezzo, M., et al.: 'Sidelobe blanking with generalized Swerling-chi fluctuation models', *IEEE Trans. Aerosp. Electron. Syst.*, 2013, **49**, pp. 982–1005
- [9] Finn, H., Johnson, R.S., Peebles, P.Z.: 'Fluctuating target detection in clutter using sidelobe blanking logic', *IEEE Trans. Aerosp. Electron. Syst.*, 1971, **7**, (1), pp. 147–159
- [10] Richards, M.A.: 'Fundamentals of radar signal processing' (McGraw-Hill, 2005, 1st edn.)
- [11] Coskun, O., Candan, C.: 'On the optimality of Maisel sidelobe blanking structure'. *Radar Conf.*, 2014 IEEE, May 2014, pp. 1102–1107
- [12] Biyari, K., Lindsey, W.: 'Statistical distributions of Hermitian quadratic forms in complex Gaussian variables', *IEEE Trans. Inf. Theory*, 1993, **39**, (3), pp. 1076–1082

- [13] Bello, P., Nelin, B.D.: 'Predetection diversity combining with selectively fading channels', *IEEE Trans. Commun.*, 1962, **10**, (1), pp. 32–42
- [14] Fernández-Plazaola, U., Martos-Naya, E., Paris, J.F., *et al.*: 'Comments on Proakis analysis of the characteristic function of complex Gaussian quadratic forms'. Computer Research Repository (CoRR), 2012, vol. abs/1212.0382
- [15] Coskun, O., Candan, C.: 'MATLAB codes for the design of Maisel sidelobe blanker systems', <http://www.eee.metu.edu.tr/~ccandan/pub.htm>
- [16] Gradshteyn, I.S., Ryzhik, I.M.: 'Table of integrals, series, and products' (Academic Press, 2007, 7th edn.), p. 709

7 Appendix

7.1 Appendix 1: Proof of optimality

Let ϕ_B and ϕ_{B^*} denote the indicator functions of Neyman–Pearson test and any other test for the blanking decision regions, respectively

$$\phi_B(\mathbf{x}) = \begin{cases} 1 & \mathbf{x} \in \text{Blank}, \quad \text{i. e. } \frac{p(\mathbf{x}; H_2)}{p(\mathbf{x}; H_1)} > \zeta \\ 0 & \mathbf{x} \in \overline{\text{Blank}}, \quad \text{i. e. } \frac{p(\mathbf{x}; H_2)}{p(\mathbf{x}; H_1)} < \zeta \end{cases}, \quad (22)$$

where $\mathbf{x} = [\tilde{s} \ \tilde{r}]$.

The following inequality immediately follows from the definitions of above expression:

$$(\phi_B - \phi_{B^*})(p(\mathbf{x}; H_2) - \zeta p(\mathbf{x}; H_1)) \geq 0. \quad (23)$$

Integrating (23) over the entire sample space, we get the following equations:

$$\begin{aligned} & \int_{\mathbf{x} \in B} (p(\mathbf{x}; H_2) - \zeta p(\mathbf{x}; H_1)) \, d\mathbf{x}, \\ & - \int_{\mathbf{x} \in B^*} (p(\mathbf{x}; H_2) - \zeta p(\mathbf{x}; H_1)) \, d\mathbf{x} \geq 0, \quad (24) \\ & P(B|H_2) - \zeta P(B|H_1) - P(B^*|H_2) + \zeta P(B^*|H_1) \geq 0, \\ & P(B|H_2) - P(B^*|H_2) \geq \zeta(P(B|H_1) - P(B^*|H_1)). \end{aligned}$$

where $P(B^*|H_2)$ and $P(B^*|H_1)$ are the probabilities of deciding blanking and not blanking for the any other test except Neyman–Pearson test.

From (24), we see that if $P(B^*|H_1) \leq P(B|H_1)$, then $P(B|H_2) \geq P(B^*|H_2)$ since $\zeta \geq 0$. Thus, any other test whose target blanking probability is desired to be upper bounded by some level will have a smaller jammer blanking probability compared with the Neyman–Pearson test.

7.2 Appendix 2: Derivation of optimum SLB detectors

7.2.1 Swerling-0 target model: We first give the conditional pdfs of \tilde{s} and \tilde{r} given that \tilde{a} and \tilde{c} are completely known. The conditional pdf will be Gaussian whose mean is reflected by target and jammer signals and is given as follows:

Under H_1 , $f(\tilde{s}|\tilde{a}; H_1) \sim \mathcal{CN}(\tilde{a}, \sigma^2)$ and $f(\tilde{r}|\tilde{a}; H_1) \sim \mathcal{CN}(\omega\tilde{a}, \sigma^2)$. Under H_2 , $f(\tilde{s}|\tilde{c}; H_2) \sim \mathcal{CN}(\tilde{c}, \sigma^2)$ and $f(\tilde{r}|\tilde{c}; H_2) \sim \mathcal{CN}(\beta\tilde{c}, \sigma^2)$. Since the conditional pdfs are in the same form, we will continue with that under H_1

$$\begin{aligned} f(\tilde{s}|\tilde{a}; H_1) &= \frac{1}{\pi\sigma^2} \exp\left(-\frac{|\tilde{s} - \tilde{a}|^2}{\sigma^2}\right), \\ f(\tilde{r}|\tilde{a}; H_1) &= \frac{1}{\pi\sigma^2} \exp\left(-\frac{|\tilde{r} - \omega\tilde{a}|^2}{\sigma^2}\right). \end{aligned} \quad (25)$$

Since the receiver noise in both channels (\tilde{w}_s and \tilde{w}_r) are assumed to be independent, \tilde{s} and \tilde{r} turns to be conditionally independent. Hence

$$f(\tilde{s}, \tilde{r}|\tilde{a}; H_1) = \frac{1}{\pi^2\sigma^4} \exp\left(-\frac{1}{\sigma^2}(|\tilde{s} - \tilde{a}|^2 + |\tilde{r} - \omega\tilde{a}|^2)\right). \quad (26)$$

Averaging (26) over the phase of \tilde{a} which is uniformly distributed over $(0, 2\pi)$, we obtain

$$\begin{aligned} f(\tilde{s}, \tilde{r}|a_0; H_1) &= \frac{1}{\pi^2\sigma^4} \exp\left(-\frac{1}{\sigma^2}(|\tilde{s}|^2 + |\tilde{r}|^2 + a_0^2 + \omega^2 a_0^2)\right) \\ & I_0\left(\frac{2a_0}{\sigma^2}|\tilde{s} + \omega\tilde{r}|\right). \end{aligned} \quad (27)$$

where $a_0 = |\tilde{a}|$ and $I_0(\cdot)$ is the modified Bessel function of the first kind. Similarly

$$\begin{aligned} f(\tilde{s}, \tilde{r}|c_0; H_2) &= \frac{1}{\pi^2\sigma^4} \exp\left(-\frac{1}{\sigma^2}(|\tilde{s}|^2 + |\tilde{r}|^2 + c_0^2 + \beta^2 c_0^2)\right) \\ & I_0\left(\frac{2c_0}{\sigma^2}|\tilde{s} + \beta\tilde{r}|\right). \end{aligned} \quad (28)$$

Then, LRT can be formed by the ratio of (28) and (27) and is given in (19).

7.2.2 Swerling-1 target model: Here, we give an alternative derivation given in [11] to optimum SLB detector for Swerling-1 target. To find the joint pdf of \tilde{s} and \tilde{r} , we integrate (27) over a_0 whose pdf is given in (6) as follows:

$$f(\tilde{s}, \tilde{r}; H_1) = \int_0^\infty f(\tilde{s}, \tilde{r}|a_0; H_1) f(a_0) \, da_0. \quad (29)$$

Putting (27) and (6) into (29), we have the following equation:

$$\begin{aligned} f(\tilde{s}, \tilde{r}; H_1) &= \frac{1}{\pi^2\sigma^4} \exp\left(-\frac{1}{\sigma^2}(|\tilde{s}|^2 + |\tilde{r}|^2)\right) \\ & \int_0^\infty \exp\left(-\frac{1}{\sigma^2}a_0^2(1 + \omega^2)\right) \\ & \times I_0\left(\frac{2|\tilde{a}|}{\sigma^2}|\tilde{s} + \omega\tilde{r}|\right) \frac{2a_0}{\sigma_a^2} \exp\left(-\frac{a_0^2}{\sigma_a^2}\right) \, da_0. \end{aligned} \quad (30)$$

One can note that

$$\int_0^\infty 2xa \exp(-ax^2) I_0(bx) \, dx = \exp\left(\frac{b^2}{4a}\right)$$

[16]. Thus, the integral in (30) can be written as

$$\begin{aligned} I &= \exp\left(\sigma_a^2 \left(\frac{|\tilde{s}|^2 + \omega^2 |\tilde{r}|^2 + 2\omega \text{Re}(s\tilde{r}^*)}{\sigma^2(\sigma_a^2(1 + \omega^2) + \sigma^2)} \right)\right) \\ & \underbrace{\left(\frac{\sigma^2}{\sigma_a^2(1 + \omega^2) + \sigma^2} \right)}_{K_1}. \end{aligned} \quad (31)$$

Putting (31) into (30), we obtain the joint pdf as

$$f(\tilde{s}, \tilde{r}; H_1) = \frac{1}{\pi^2\sigma^4} \exp\left(-\frac{1}{\sigma^2}(|\tilde{s}|^2 + |\tilde{r}|^2)\right) \times I. \quad (32)$$

Similarly, one can find joint pdf of \tilde{s} and \tilde{r} under H_2 . Note that K_1 term does not involve data and K_2 term is common for both hypotheses. After some algebraic manipulations, the LLRT can be found as given in (9).

7.2.3 Swerling-3 target model: Using the same method in Swerling-1 case, the joint pdf of \tilde{s} and \tilde{r} under H_1 can be found by integrating (27) over a_0 whose pdf is given in (20). Then

$$\begin{aligned}
f(\tilde{s}, \tilde{r}; H_1) &= \frac{1}{\pi^2 \sigma^4} \exp\left(-\frac{1}{\sigma^2}(|\tilde{s}|^2 + |\tilde{r}|^2)\right) \\
&\int_0^\infty \exp\left(-\frac{1}{\sigma^2} a_0^2 (1 + \omega^2)\right) \\
&\times I_0\left(\frac{2|\tilde{a}|}{\sigma^2} |\tilde{s} + \omega \tilde{r}|\right) \frac{8a_0^3}{\sigma^4} \exp\left(-\frac{a_0^2}{\sigma^2}\right) da_0.
\end{aligned} \tag{33}$$

By making use of the relation

$$\int_0^\infty 2x^3 \exp(-ax^2) I_0(bx) dx = \frac{1}{a^2} \left(1 + \frac{b^2}{4a}\right) \exp\left(\frac{b^2}{4a}\right)$$

and after some straightforward algebra the joint pdf of \tilde{s} and \tilde{r} under H_1 can be written as [16]

$$f(\tilde{s}, \tilde{r}; H_1) = K_1 K_2 \exp(-\mathbf{x}^H \mathbf{C}_1^{-1} \mathbf{x}) (1 + \mathbf{x}^H (-\mathbf{C}_1^{-1} + \mathbf{I}) \mathbf{x}). \tag{34}$$

where \mathbf{I} is identity matrix, K_1 and K_2 are defined in (31) and (33), respectively. Similarly, $f(\tilde{s}, \tilde{r}; H_2)$ can be found by replacing \mathbf{C}_1 in (34) by \mathbf{C}_2 . Then, the LLRT can be found as given in (21).